Global and Planetary Change **42** (1–4), 59–81, 2004
http://www.elsevier.com/locate/gloplacha
— Authors' final version —

Simulation of the Eurasian ice sheet dynamics during the last glaciation

Pirjo-Leena Forsström (1) and Ralf Greve (2)

(1) CSC – Scientific Computing Ltd., P.O. Box 405,
FIN-02101 Espoo, Finland

(2) Institute of Low Temperature Science, Hokkaido University,
Kita-19, Nishi-8, Kita-ku, Sapporo 060-0819, Japan

January 15, 2004

Correspondence to: P.-L. Forsström (forsstro@csc.fi)

Abstract

The Eurasian Weichselian glaciation is studied with the SICOPOLIS ice-sheet model and UKMO PMIP climate anomaly forcings. A set of sensitivity tests are completed, including runs in cold-ice mode, different positive-degree-day (PDD) factors and modified climatic data-sets. The model set-up with present-day climatology modified by a glacial index brings forth an areally correct Last Glacial Maximum (LGM) extent in the western areas, but the ice-sheet volume is too small compared to reconstructions from rebound rates. Applying modified climate data results in similar extent as indicated by the Quaternary Environment of the Eurasian North (QUEEN) Late Weichselian ice-sheet reconstruction. The simulation results display freshwater fluxes from melting and calving in phase with Heinrich events H3 at 27, H2 at 22, and H1 at 14 ka ago. These peaks correspond to fast flow areas, with main activity at 27 and 22 ka ago in the Nordic Channel area and later in the Bear Island and Storfjorden region. The activity of these areas seems to be shifting from south to north from LGM to the Holocene. The freshwater pulse at 19–18.5 ka could correspond to Dansgaard-Oeschger oscillation, as well as ice volume flux peaks around 18–17 ka ago on the western margin of the ice sheet.

1 Introduction

The Weichselian period is characterized by huge ice sheets in the northern hemisphere (Peltier, 1994). Many reconstructions have been made of Eurasian ice-sheet extent, the most complete one was compiled by the Quaternary Environment of the Eurasian North (QUEEN) project (Svendsen et al., 1999; Thiede et al., 2001). This reconstruction differs form earlier compilations especially in the Southern Kara Sea and the Taymyr Peninsula area, which are deduced to have been ice-free during the Last Glacial Maximum (LGM) around 20 ka ago (Svendsen et al., 1999; Polyak et al., 2000; Mangerud et al., 2002). A correct understanding of ice-sheet extent and flow is linked closely to our understanding of the Eurasian paleoclimate. Here, both topics will be exploited using a numerical model driven by various climatologies. Our goal is to reconstruct ice sheet extent, volume, and flow according to best glacial-geologic records.

The timing of the glacial maxima vary across Eurasia. In the western section, the Scandinavian ice sheet (SIS) and the British Isles ice sheet (BIIS) developed. In the north in the Barents Sea and the Arctic islands the Barents ice sheet (BIS) and in the east the controversial Kara ice sheet (KIS) developed. From the QUEEN summary, the timing of the LGM is given in Table 1.

Western section	Central section	Eastern section
25–22 ka ago	19–17 ka ago	28–20 ka ago

Table 1: Timing of maximum ice extent for different sectors.

The maximum position in the west was a late, short event at 25 ka ago, the decay starting around 22–20 ka ago. The eastern SIS grew to maximum extent at 19–17 ka ago, and then started to retreat. The retreat stopped at Salpausselka I at 12 ka ago (Saarnisto and Lunkka, 2002). The BIS started to retreat at 15 ka, and deglaciation was completed by 10 ka ago. In this paper, we refer to the LGM as the coldest time of the simulation period.

Direct proxies for local temperature and precipitation during the LGM are rare. Where records do exist, they derive from paleobotanical evidence (Tarasov et al., 1999; Peyron et al., 1998). Regional records, from Greenland ice cores and deep-sea sediments, are also of use in bridging local observations and driving and testing paleoclimate models. Kageyama et al. (2001) have reconstructed LGM climate using all available proxies and compared their reconstructions to the output climate data-sets from the Paleoclimate Modelling Intercomparison Project (PMIP). Significant differences were noted in two main regions, southwestern Europe, where the PMIP results are too warm with too much precipitation, and the northern parts of European Siberia, where the results for summer temperatures are too cold. Especially, if these reconstructions are compared to PMIP results from the United Kingdom Meteorological Office (UKMO) (Hewitt and Mitchell, 1997), we can see that the winter temperature anomaly in southeast regions is in agreement with the results obtained by Tarasov et al. (1999). However, the UKMO results show an anomaly of similar magnitude in the northeast, whereas Tarasov et al. (1999) state that the temperatures at LGM were warmer. The UKMO21 PMIP results indicate an anomaly in precipitation and temperatures, as shown in Fig. 1.

Early Weichselian conditions are also of concern: Pollard and Barron (2003) simulate the oxygen-isotope stage 3 (OIS3), based on nesting a high-resolution mesoscale model (RegCM2, Giorgi et al., 1993a,b) for Europe within a general circulation model (GENESIS GCM, Thompson and Pollard, 1997), and find north Atlantic sea-surface temperatures and hence the ice-sheet size to be the key to a very cold European continent.

Ice sheet models exploit proxy and reconstructed climate data. To reconstruct the glaciation, simulations of Northern Hemisphere ice-sheet retreat using atmospheric general circulation model (AGCM) results have been carried out by Charbit et al. (2002), and by Marshall et al. (1999) and Marshall and Clarke (1999) for the Laurentide and Greenland ice sheets. Scandinavian and related ice sheets have been simulated by Fastook and Holmlund

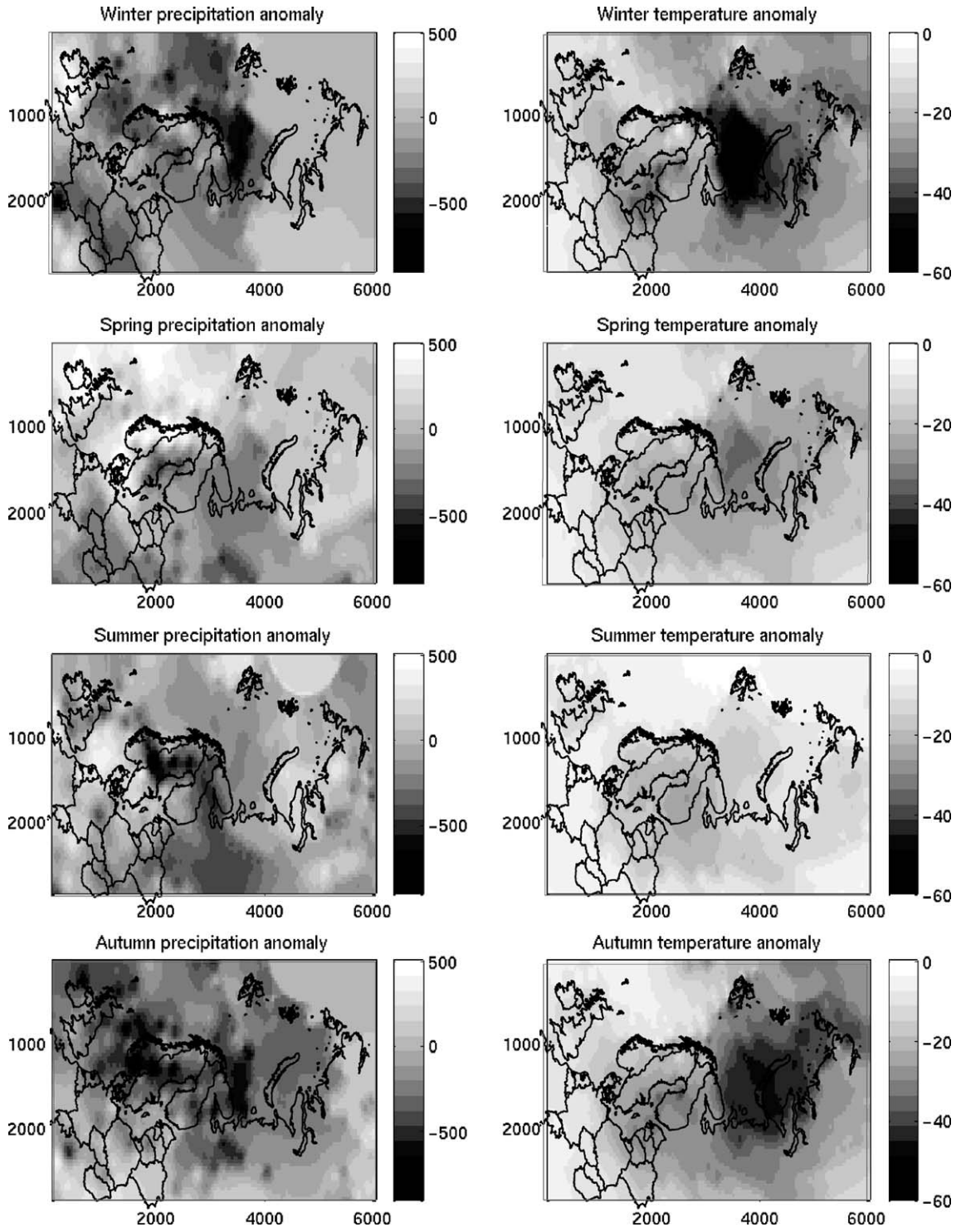

Figure 1: Anomalies for precipitation (left panel, in mm year^{-1}) and temperature (right panel, in °C) at the LGM defined by UKMO21 simulation results. Areal coverage is $6040 \times 2840\,\mathrm{km}^2$ in the stereographic plane. Axis units are in km.

(1994), Peltier (1994), Huybrechts and T'siobbel (1995), Payne and Baldwin (1999) and Siegert et al. (1999).

Several lines of evidence indicate fast ice-stream flow in paleo-ice-sheets of the Northern Hemisphere. Distinct pulses of ice-rafted debris (IRD) in deep-sea sediments have been interpreted to represent rapid discharge events through ice streams (Bond et al., 1992). Glacial geologic features also support the existence of ice streams, in both North American and Eurasian ice sheets. For example, the Scandinavian ice-sheet dynamics is characterized by several major ice streams (Stokes and Clark, 2001; Boulton et al., 2001). The Norwegian Channel Ice Stream (NCIS) has been identified from geological data (e.g., glacially fed fans) (Sejrup et al., 1998, 2000), the Baltic Ice Stream and its sublobes have been discussed (e.g., Kleman et al., 1997) and the Finnish, the Karelian and the Novgorod ice streams are studied by, e.g., Kjaer et al. (2001), Larsen et al. (1999) and Lunkka et al. (2001). In the North, ice streams were located at Saint Anna Trough, Franz Victoria Trough, Bear Island Trough and Storfjorden Trough (Sejrup et al., 2000; Knies et al., 2001). These ice streams transported ice to the calving area. The fast ice-sheet flow associated with large flux events will remove basal ice, and thus basal debris, by frictional melting. This basal debris entrained in calved icebergs is sedimented to the ocean as the icebergs melt.

The marine record of glacial-age northern ocean is punctuated by IRD events. The long-term cooling trends (Bond cycles) are terminated by Heinrich Events (HEs) (Heinrich, 1988; Bond and Lotti, 1995). Dansgaard-Oeschger (D-O) oscillations are superimposed upon these (Dansgaard et al., 1982). The HEs are associated with a temperature decrease recorded by ice core isotopes and low sea-surface temperatures in North Atlantic sediment cores (Bond et al., 1993). Heinrich events seem especially to have a connection to the Laurentide ice-sheet dynamics (Alley and Clark, 1999; Calov et al., 2002). The timings of HEs from Elliot et al. (1998) are represented in Table 2.

HE	Pos.	Age (ka)
H1	Base	15.1
	Top	13.4
H2	Base	22.1
	Top	20.4
H3	Base	27.7
	Top	25.1

Table 2: Average age and duration of the HEs (Elliot et al., 2001). The base and top values refer to HE start (base) and end (top) in ocean sediment cores from the North Atlantic.

Dansgaard-Oeschger temperature oscillations can be grouped as warm-cold oscillations, with increasingly cold minima, until a very warm maximum. After this culmination (HE),

the oscillation cycle begins again (Heinrich, 1988; Dansgaard et al., 1982, 1993; Clark et al., 1999; Alley and Clark, 1999; Stocker, 2000). They occur more frequently than the HEs, and are centered on the Northern Atlantic. The D-O oscillations are reflected as detrital events in sediment cores with varied petrology, associated with changing iceberg source area (Bond and Lotti, 1995) and different paleo-ice streams. A compilation of the D-O oscillations is given in Table 3, with the numbering applied by Bond and Lotti (1995).

D-O	Age (ka)
a	15.9
b	17.3
c	19.0
d	23.3
e	24.5

Table 3: Results of D-O oscillations and timing for core Na87-22 (Elliot et al., 1998).

There is an ongoing debate on the evolution of climatic events around the HEs and the D-O maxima (see, e.g., Clark et al., 2002). The meltwater pulses from ice sheets affecting the thermohaline circulation, temperatures and salinity are thought to be a significant factor in the climatic interactions. Ganopolski and Rahmstorf (2001) show that warm events, like the D-O maxima, can be triggered by a small perturbation in freshwater flux to the Nordic Seas. At least two meltwater pulses appear to have occurred during the deglaciation: the melt-water pulse IA (mwp-IA) and IB (mwp-IB) (Koç and Jansen, 1992). These are timed at 13.5 and 9.5 ka ago, respectively. The corresponding estimated meltwater discharges from all continental ice sheets are 14000 and 9000 km^3, respectively (Fairbanks, 1989). If the volume of the Scandinavian ice sheet at those dates was 1/3 and 1/4 of the total northern hemisphere ice volume (Peltier, 1994), then their corresponding share of SIS meltwater production were 4700 and 2300 km^3.

The record of cores located near the Scandinavian coast show well-defined IRD-layers with sharp bottom and top boundaries (Elliot et al., 2001). These records also indicate that HEs are characterized by nearly synchronous deposits on all locations, and that inter-HEs show synchronous increase only in the Norwegian Sea area. The IRD records also exhibit a change in regime between 20 and 13 ka ago.

2 Modelling approach

We are using a thermodynamical ice sheet model to investigate the Eurasian ice sheet mass balance and geographic extent, with a particular interest in calving margin discharge. This is realised by the ice-sheet model SImulation COde for POLythermal Ice

Sheets (SICOPOLIS; Greve, 1997a,b). It is based on the continuum-mechanical balance equations and jump conditions of mass, momentum and energy. The model treats ice as an incompressible, heat-conducting, power-law fluid with thermo-mechanical coupling due to the strong temperature dependence of the flow law:

$$\boldsymbol{D} = EA(T', \omega)\sigma^{n-1}\,\boldsymbol{t}^{\mathrm{D}}, \tag{1}$$

where $\boldsymbol{D} = \mathrm{sym\,grad}\,\boldsymbol{v}$ (velocity $\boldsymbol{v}$) is the strain-rate tensor, $\boldsymbol{t}^{\mathrm{D}}$ the Cauchy stress deviator, $\sigma = [\mathrm{tr}\,(\boldsymbol{t}^{\mathrm{D}})^2/2]^{1/2}$ the effective shear stress, n the power-law exponent and $A(T', \omega)$ the flow-rate factor, which depends exponentially on the temperature T' relative to the pressure melting point and linearly on the water-content ω (see Greve et al., 1998). The flow-enhancement factor E is equal to unity for pure ice and can deviate from unity due to the softening or stiffening effect of impurities in the ice. Values of the physical model parameters are listed in Table 4.

Quantity	Value
Gravity acceleration, g	$9.81\,\mathrm{m\,s^{-2}}$
Density of ice, ρ	$910\,\mathrm{kg\,m^{-3}}$
Power-law exponent, n	3
Flow-enhancement factor, E	3
Heat conductivity of ice, κ	$9.828\,e^{-0.0057\,T[\mathrm{K}]}\,\mathrm{W\,m^{-1}\,K^{-1}}$
Specific heat of ice, c	$(146.3 + 7.253\,T[\mathrm{K}])\,\mathrm{J\,kg^{-1}\,K^{-1}}$
Latent heat of ice, L	$335\,\mathrm{kJ\,kg^{-1}}$
Clausius-Clapeyron gradient, β	$8.7 \times 10^{-4}\,\mathrm{K\,m^{-1}}$
Geothermal heat flux, q_{geo}	$55\,\mathrm{mW\,m^{-2}}$
Threshold seabed elevation for glaciation, z_{thresh}	$-500\,\mathrm{m}$
Isostatic time lag, τ_{iso}	3000 years
Asthenosphere density, ρ_{a}	$3300\,\mathrm{kg\,m^{-3}}$
Density $\times$ specific heat of the lithosphere, $\rho_{\mathrm{r}} c_{\mathrm{r}}$	$2000\,\mathrm{kJ\,m^{-3}K^{-1}}$
Heat conductivity of the lithosphere, κ_{r}	$3\,\mathrm{W\,m^{-1}\,K^{-1}}$

Table 4: Physical parameters of the ice-sheet model.

SICOPOLIS is based on the shallow-ice approximation (SIA), that is, normal stress deviators and shear stresses in vertical planes are neglected. The large-scale behavior of ice sheets is simulated well with the SIA; however, it is not valid locally in the vicinity of ice domes and close to the margin. SICOPOLIS can produce fast-flow due to sliding over a temperate ice base (Eq. (2)). These fast-flow features resemble ice streams, but

as no specific ice-stream dynamics is included, they are a coarse approximation of the real dynamics. Ice shelves are not treated explicitly. Instead, the ice sheet is allowed to glaciate the continental shelf below sea level, provided the seabed elevation is larger than a given threshold value z_{thresh} (Forsström et al., 2003). Elsewhere, the ice sheet thickness is set to zero, which may be interpreted as a simple model for calving, and might lead to underestimated calving rates.

The model discerns *cold ice*, with a temperature below the pressure melting point, and *temperate ice*, with a temperature at the pressure melting point. Temperate ice is considered as a binary mixture of ice and small amounts of water. The interface that separates cold and temperate ice is monitored using Stefan-type energy flux and mass flux matching conditions. The general assumption is that the water content in temperate zones of polythermal ice sheets is small (Hutter, 1993). Basal sliding is assumed to be zero for a cold base, and for a temperate base it is described by the Weertman-type sliding law in the form of Greve et al. (1998):

$$\boldsymbol{v}_{\mathrm{sl}} = -C_{\mathrm{sl}} H \|\mathrm{grad}\, h\|^2\, \mathrm{grad}\, h, \tag{2}$$

where $\boldsymbol{v}_{\mathrm{sl}}$ is the basal sliding velocity, C_{sl} the sliding coefficient, H the ice thickness and h the surface elevation.

The model computes the three-dimensional evolution of ice extent, thickness, velocity, temperature and water content in the temperate ice region and age in response to external forcings. The forcings due to climate and heat from Earth's interior, are: (1) the mean annual air temperature at the ice surface; (2) the surface mass balance, which is ice accumulation (here assumed to be snowfall) minus ablation (here assumed to be melting); (3) the global sea level; and (4) the geothermal heat flux entering the ice mass from below. Surface processes like refreezing are accounted for. Sea level changes were derived from the SPECMAP record (Imbrie et al., 1984) and the global-mean value $q_{\mathrm{geo}} = 55\,\mathrm{mW\,m^{-2}}$ is used for the geothermal heat flux.

The model tracts freshwater production by: (1) melting and calving; (2) water drainage due to basal melt; and (3) surplus water drainage from temperate layers. As there is no specific calving law included, ice arriving at the coast is converted into freshwater. There is no distinction between surface melt (which is assumed to run off instantaneously) and calving in the model results for freshwater production, so that at every time-step, melting as well as calving anywhere on the surface is summed up to the total volume of freshwater release into the ocean. The water flux into the ice-sheet base is generated from melting basal ice. The causes for melting are the geothermal heat flux and basal frictional heating from sliding over the bed. The water storage capacity of temperate ice is assumed to have

an upper limit, above which surplus water is drained instantaneously into the ground. No model for basal water flow or storage in the ground is included. This would not be an easy task, as the current knowledge about basal conditions and melting is limited. Models and some observations of bed properties (Engelhardt and Kamb, 1997; Hulbe and MacAyeal, 1999; Huybrechts and de Wolde, 1999) indicate that basal melting has a strong control on ice flow (see also Blankenship et al., 1993; Fowler and Johnson, 1995; Raymond, 2000; Tulaczyk et al., 2000a,b). The best method to include basal water would be to couple the depth of basal water with the sliding laws (Johnson and Fastook, 2002).

Isostatic depression and rebound of the lithosphere due to changing ice load is described by a local-lithosphere-relaxing-asthenosphere (LLRA) model with an isostatic time lag τ_{iso} (LeMeur and Huybrechts, 1996; Greve, 2001). A more detailed description of the model is given by Greve (1997a,b). The geographical area in our simulations extends from the Northern Atlantic to the Taymyr Peninsula, and covers an area of $6040 \times 2840\,\text{km}^2$. The domain was chosen to include both the British Isles and the eastern section of the Eurasian ice sheet. The area includes the Alps in the south, the Ural and the highlands of Taymyr and Tunguska. A stereographic projection with a reference latitude of 71° is used. The model domain grid spacing for all vertical regions is 40 km in the horizontal, leading to a total of 151×71 grid points. The distortion arising from the projection is accounted for by introducing the corresponding components of the orthogonal metric tensor in all terms with horizontal derivatives in model equations. The vertical resolution is 21 grid points in cold-ice region, 11 grid points in temperate-ice region (if existing) and 11 grid points in the lithosphere (Greve, 1997a).

The model is initialized in an ice-free state, 250 ka ago. Climate conditions are tied to the Greenland ice core record. Thus, the simulation runs through one complete glaciation and deglaciation before the time period discussed in this article. The forcing method for is discussed in detail in Section 3.

3 Climatic forcing

The description of a time-evolving climatology is essential for the simulation of ice-sheets through glacial cycles. This can be done in several ways. The most sophisticated solution would be to connect a climate model and the ice-sheet model, but this is computationally very costly. A general solution is to use snapshots of climate, produced by climate models. We are using the anomaly of temperature and precipitation, resulting from a climate model run, scaled by a glaciation index, in which maximum glacial conditions are those at the LGM and maximum interglacial conditions are those of the present-day.

Modern surface temperature and precipitation values are from the measured and modelled data sets by Legates and Wilmott (1990). These data sets have been gathered from the Global Historical Climatology Network (Vose et al., 1992) and station records from the years 1950 throughout 1996. The source resolution is $0.5° \times 0.5°$, and the data are interpolated for each season with inverse-distance weighing to the 40-km grid of SICOPOLIS. The surface elevation data is from the ETOPO5 data-set and is also interpolated to our coarser grid.

LGM climate conditions, temperature and precipitation, and elevation derive from the UKMO LGM simulations (Hewitt and Mitchell, 1997) are utilized. The UKMO21 data-set was chosen from comparisons of ice-sheet mass budgets in the Paleoclimate Modeling Intercomparison Project (PMIP) simulations (Pollard and PMIP Participating Groups, 2000).

3.1 First set-up ("primary approach")

A simple approach is to interpolate seasonal climate variables linearly between the present and LGM conditions. Forsström et al. (2003) use a glaciation index $g(t)$, that scales the GRIP δ^{18}O record (Dansgaard et al., 1993) to represent LGM ($g = 1$) and present ($g = 0$) conditions (Fig. 2). Here, we refine this approach by defining anomalies:

$$f_{\mathrm{anom}}(x, y) = f_{\mathrm{LGM}}^{\mathrm{UKMO}}(x, y) - f_{\mathrm{present}}^{\mathrm{UKMO}}(x, y), \tag{3}$$

where x and y are Cartesian coordinates which span the stereographic plane, t is the time, f is the surface temperature or precipitation (Fig. 1) and $f_{\mathrm{present}}^{\mathrm{UKMO}}(x, y)$ and $f_{\mathrm{LGM}}^{\mathrm{UKMO}}(x, y)$ are the spatially resolved data for the two time-slices, respectively. The temperature or precipitation at any time t is then calculated based on the Legates and Wilmott (L&W) data-sets for modern precipitation and temperature:

$$f(x, y, t) = f_{\mathrm{present}}^{\mathrm{L\&W}}(x, y) + g(t)\, f_{\mathrm{anom}}(x, y), \tag{4}$$

where $f_{\mathrm{present}}^{\mathrm{L\&W}}(x, y)$ and $f_{\mathrm{LGM}}^{\mathrm{L\&W}}(x, y)$ are the spatially resolved data for the two time-slices, respectively. This approach is referred to as the *primary approach* in the following text.

We could also have used the UKMO 6 ka results as an additional reference state, but as the Eurasian ice sheets had melted before that time period, the usefulness of it would be questionable. Here, the best glacial index zero-reference level is the present-day climate, as direct measurements of the climate parameters are available.

Seasonal precipitation P must be converted to snowfall (solid precipitation) S. This is

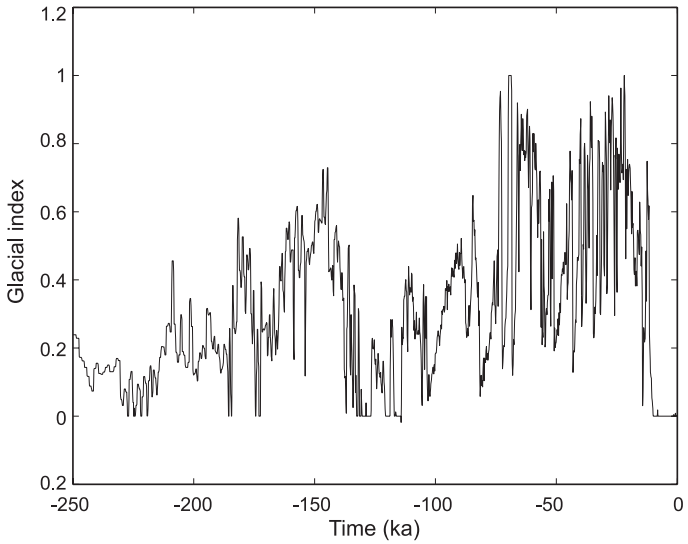

Figure 2: Glacial index $g(t)$ as a function of time. This index scales the GRIP δ^{18}O record (Dansgaard et al., 1993) to represent glacial ($g = 1$) and present ($g = 0$) conditions.

accomplished using Marsiat's (1994) empirical relation:

$$S = P \times \begin{cases} 0, & T_\mathrm{s} \geq 7^\circ\mathrm{C}, \\ (7^\circ\mathrm{C} - T_\mathrm{s})/17^\circ\mathrm{C}, & -10^\circ\mathrm{C} \leq T_\mathrm{s} \leq 7^\circ\mathrm{C}, \\ 1, & T_\mathrm{s} \leq -10^\circ\mathrm{C}, \end{cases} \tag{5}$$

where T_s represents the seasonal surface temperature.

Surface melting must also be estimated. Our primary approach follows Reeh's (1991) form of the degree-day method using temperatures as defined in Eqs. (3) and (4). For the degree-day factors, which describe the increase of ablation with increasing surface temperature (Reeh, 1991). The parameters used here were the degree-day factor for snow melt, $\beta_\mathrm{snow} = 3\,\mathrm{mm\,w.e.\,day^{-1}\,^\circ C^{-1}}$, degree-day factor for ice melt, $\beta_\mathrm{ice} = 7\,\mathrm{mm\,w.e.\,day^{-1}\,^\circ C^{-1}}$, saturation factor for the formation of superimposed ice $P_\mathrm{max} = 0.6$, and a standard deviation of short-term, statistical air-temperature fluctuations of $\sigma_\mathrm{stat} = 5^\circ$C. Variations of these values are discussed below.

With the anomaly method, errors in computed present and past climate parameters are assumed to cancel each other. Other sources of error include processes like feed-back effects due to changed ice sheet topography, the calving law and unified ablation coefficients. The degree-day model, which relates the melting rate to the air-temperature excess above the melting point, does not account for the influence of wind speed, albedo and cloud cover. Utilising an energy-balance model (Braithwaite, 1995) would improve the surface melting calculations. To evaluate our model sensitivity, we have conducted several runs to study the influence of parameterizations and forcing data sets. In these runs we studied the effect

of different climate data sets, cold and polythermal mode and different positive-degree-day (PDD) factors, described in detail below.

3.2 Modified PDD factors

PDD calculations are sensitive to variations in air temperature. A small increase in climate variability can have large effects on meltwater production (Van der Veen, 1999). Various authors use a range of degree-day factors. Braithwaite (1995) asserts that at low temperatures, even values of $\beta_{\text{ice}} = 20\,\text{mm w.e. day}^{-1}\,^{\circ}\text{C}^{-1}$ are realistic. For snow, he estimates the ablation factor to be in the range of $\beta_{\text{snow}} = 3 \ldots 5\,\text{mm w.e. day}^{-1}\,^{\circ}\text{C}^{-1}$. Hagen et al. (1999) use the values $\beta_{\text{snow}} = 2.9\,\text{mm w.e. day}^{-1}\,^{\circ}\text{C}^{-1}$ and $\beta_{\text{ice}} = 4.6\,\text{mm w.e. day}^{-1}\,^{\circ}\text{C}^{-1}$ for Svalbard, and $\beta_{\text{snow}} = 4.1\,\text{mm w.e. day}^{-1}\,^{\circ}\text{C}^{-1}$ and $\beta_{\text{ice}} = 7\,\text{mm w.e. day}^{-1}\,^{\circ}\text{C}^{-1}$ for Norway. We test the model sensitivity to β_{ice} with extreme values of $5\,\text{mm w.e. day}^{-1}\,^{\circ}\text{C}^{-1}$ to $12\,\text{mm w.e. day}^{-1}\,^{\circ}\text{C}^{-1}$. The snow-melt factor is not varied due to its smaller influence on computed melt rates.

3.3 Modified precipitation and temperature data

Prior experience suggests that our primary model set-up may lead to an incorrect estimate of ice mass and ice-sheet extent in the eastern section. This is because the PMIP UKMO runs use the ice-sheet configuration of ICE4G by Peltier (1994), which, according to QUEEN project results, is too extensive in the eastern sector. QUEEN-based GCM LGM runs produce precipitation-rate anomalies of $-200\,\text{mm year}^{-1}$ in the northeast and $-400\,\text{mm year}^{-1}$ in the southeast part. As we do not have complete GCM results based on the QUEEN extent yet, we modify the above-defined precipitation anomalies instead.

Two alternative climate scenarios are tested. In the first, the precipitation anomaly in the eastern sector of the model domain was set to a value between 0 and $-400\,\text{mm}$, depending on the season (Fig. 3). In the second, the LGM temperature anomalies according to Kageyama et al. (2001) are applied. This data is presented on a coarser grid, so the interpolated values were smoothed with a convolution filter. Anomalies with the coldest temperatures are assigned to the winter months (December, January, February), and those with the warmest temperatures are assigned to the summer months (June, July, August). Spring (March, April, May) and autumn (September, October, November) values are interpolated form the winter and summer as:

$$f_{\text{anom}}^{\text{mam}} = f_{\text{anom}}^{\text{son}} = \frac{f_{\text{anom}}^{\text{djf}} + f_{\text{anom}}^{\text{jja}}}{2}. \tag{6}$$

The modified temperature and precipitation anomalies are depicted in Fig. 4.

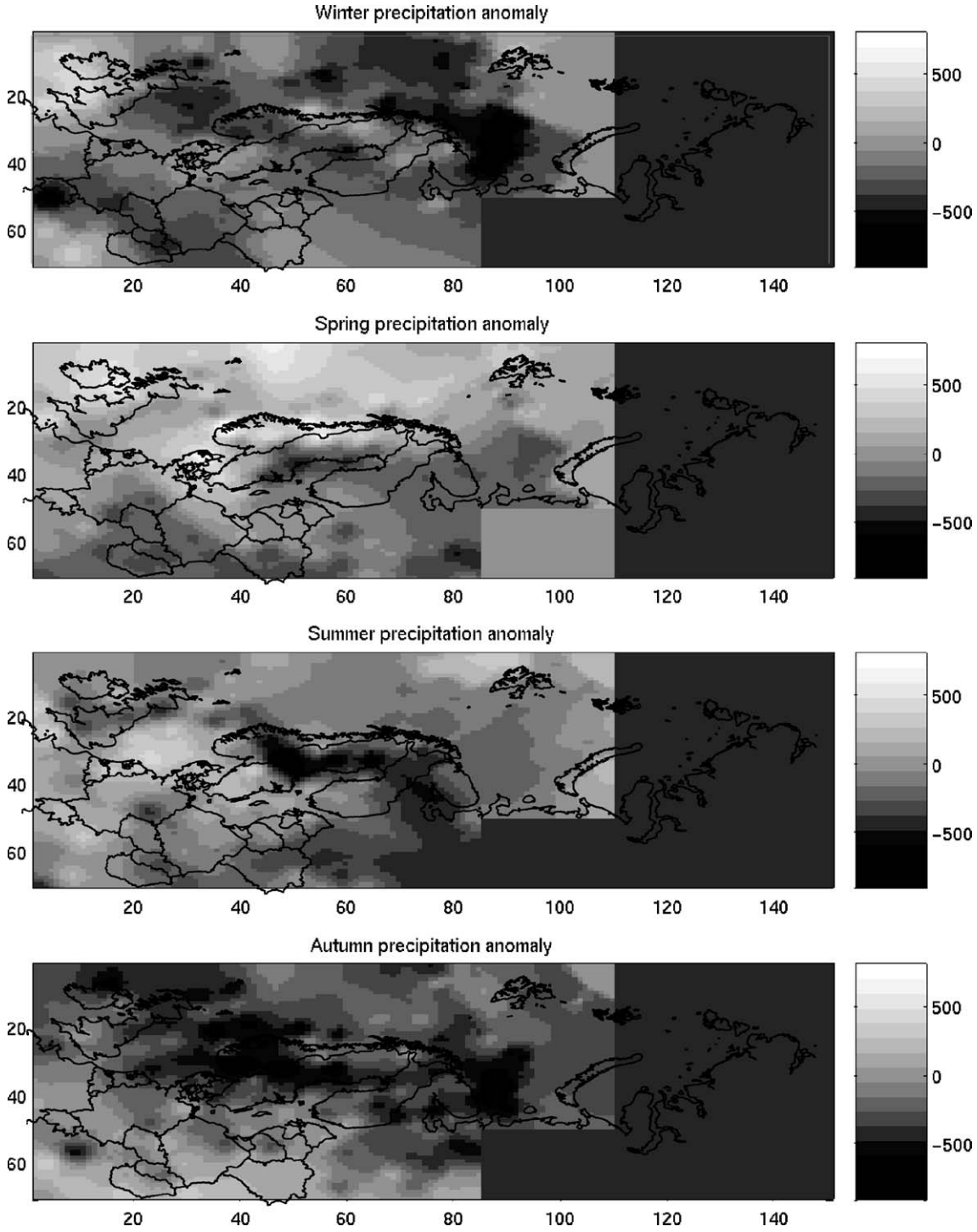

Figure 3: Anomalies for precipitation (in $\mathrm{mm\,year^{-1}}$) at the LGM, with the UKMO PMIP data modified in the eastern part of the model domain. Areal coverage is $6040 \times 2840\,\mathrm{km}^2$ in the stereographic plane. Axis units are in km.

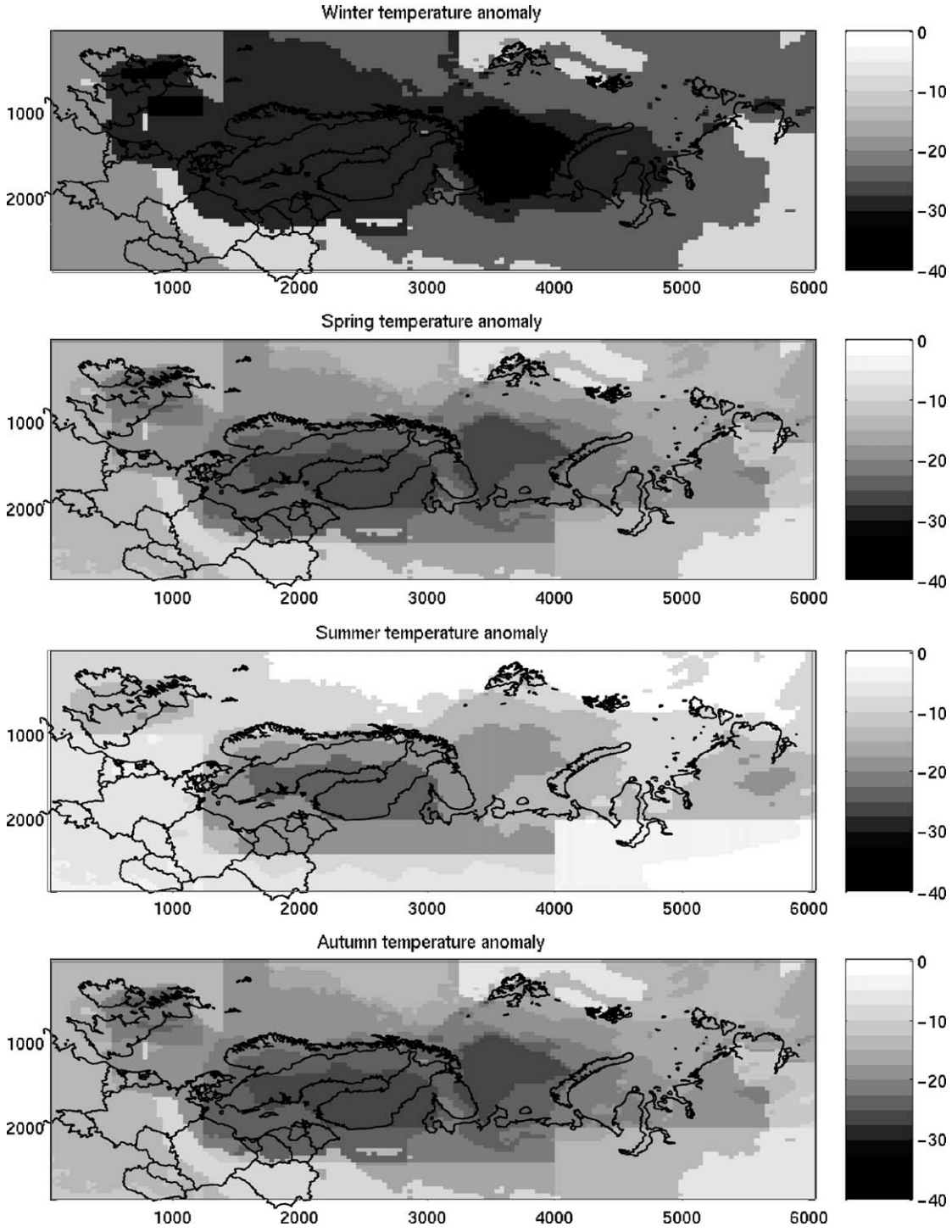

Figure 4: Anomalies for temperature (in °C) at the LGM modified from results by Kageyama et al. (2001). Areal coverage is $6040 \times 2840\,\mathrm{km}^2$ in the stereographic plane. Axis units are in km.

4 Ice sheet simulations

Ice sheets computed using the primary and modified forcings differ in both extent and volume. The more pronounced difference is in configuration (ice extent). The freshwater production curve has similarly timed peaks in all runs, but magnitudes vary. Ice-stream activity also varies among models. In the following discussion we present results of the primary approach and then make comparisons with a modified-precipitation (Eq. (6)) and with modified PDD models. Table 5 gives an overview of the different simulations.

Simulation	Set-up
#1	primary approach (as defined in Section 3.1)
#2	cold-ice mode
#3	β_{ice} reduced to 5 mm w.e. day^{-1} °C^{-1}
#4	β_{ice} increased to 12 mm w.e. day^{-1} °C^{-1}
#5	reduced LGM precipitation in the east
#6	LGM anomalies based on Kageyama et al. (2001)

Table 5: Set-up for the simulations discussed in this study.

4.1 The primary approach (simulation #1)

The primary model configuration produces a relatively expansive LGM ice sheet in the east while relatively little glacial ice forms in the western-most region of the model domain (Fig. 5, solid line). The northern Arctic islands are covered by extensive ice masses, and the Yamal and Taymyr Peninsulas are glaciated. The Barents ice sheet extends in the east to the Novaya Zemlya coast, with a maximum surface elevation of 2 km. The ice sheet has a maximum areal extent at 22 ka ago, when the lowlands to the south of the main ice domes are covered by a few hundred meters of ice. The BIIS appears as a modest few hundred meters of ice, covering Scotland and North Ireland for some 1000 years around the LGM.

At the LGM, the Barents ice sheet does not cover the whole Barents Sea area. For example, the sea north of the Kolan Peninsula is ice-free. This is due to the precipitation anomaly defined by the PMIP output: the central areas of the ice sheet are dry. The precipitation is forced with the glacial index, but the real change in precipitation in the area is apparently not that simple. The simulated SIS is two-domed. One dome is centered in the Norwegian highlands and the other in Fenno-Karelia. The maximum surface elevation for both is about 2 km.

The evolution of the glaciation from 22 ka ago to the present is depicted in the upper row of Fig. 6. The main ice sheet domes grow between the LGM and 18 ka ago, even

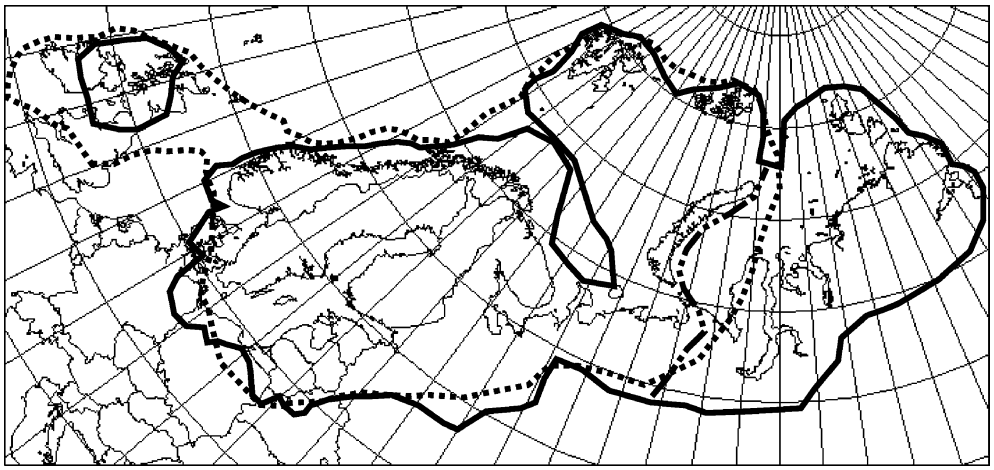

Figure 5: Ice extent at 22 ka ago (LGM) for simulations #1 (primary approach, solid line), #5 (reduced LGM precipitation, dash-dotted line) and #6 (Kageyama anomalies, dotted line). The result of simulation #5 follows that of #1 where the dash-dotted line is not visible.

as the areal extent decreases. After that time, the SIS and southeastern sector rapidly disintegrate. The cooling at 12 ka ago causes a short, modest glaciation of Scandinavian areas. Thereafter, the SIS disappears and only the BIS remains. By 9 ka ago, all ice has disappeared from the area.

The effects of model-simulated fast ice flow are readily apparent in the ice sheet topography. Relatively rapid draw-down produces troughs. The troughs form in regions identified as sites of paleo ice-stream flow. This is discussed in detail by Forsström et al. (2003).

Fig. 7 summarises some of the simulated parameters during the evolution of the Eurasian glaciation. The ice volume varies along with the glaciation index. Before the LGM, there are smaller peaks in volume around 60 and 35 ka ago. Near the LGM, ice-sheet volume peaks at 22 ka ago ($7.3 \times 10^6\,\mathrm{km}^3$) and 19 ka ago ($8.1 \times 10^6\,\mathrm{km}^3$). From that time on, the ice sheet declines, with temporary hiatuses at 16–14 ka ago and 12–11 ka ago. The maximum volume at 19–18 ka ago is an exception to the otherwise synchronous trends in ice volume and glaciation index: the ice volume grows as temperatures are on the rise. This growth is concentrated on the domes mentioned earlier, and is probably caused by an increased precipitation accompanying climate warming.

Deglaciation starts in Scandinavia, and the SIS is the first ice sheet to disappear. The BIS disintegration is sluggish, until all ice has vanished by 9.0 ka ago.

The volume of temperate ice is, in general, closely connected to the total volume of the ice sheet. The volume of temperate ice shows several peaks in the simulation: at 35 ka ago ($75 \times 10^3\,\mathrm{km}^3$), 27 ka ago ($90 \times 10^3\,\mathrm{km}^3$), 23–22 ka ago ($140 \times 10^3\,\mathrm{km}^3$), 20–19 ka ago

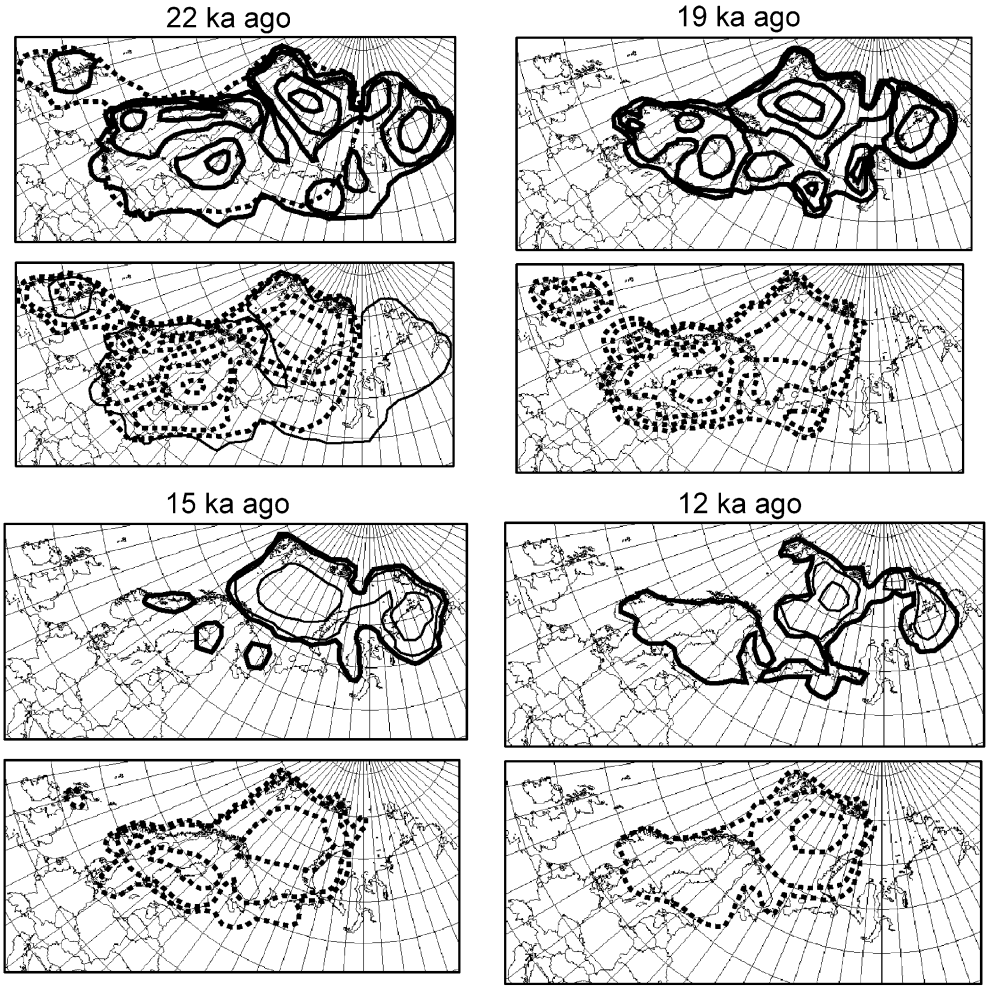

Figure 6: Topographic evolution resulting from simulations #1 (primary approach; upper panels, solid contours) and #6 (Kageyama anomalies; lower panels, dotted contours) at 22, 19, 15 and 12 ka ago. Contour spacing is 1 km.

($60 \times 10^3\,\mathrm{km}^3$) and 12 ka ago ($15 \times 10^3\,\mathrm{km}^3$). The peak at 19–18 ka ago is unusual, as it is much smaller as it would have been expected from the total volume. The cause for this is presumably the large surface accumulation on the ice domes, leading to suppression of temperatures. Larger areal extent coincides with larger areas of temperate ice at the base. This is evident, as the flow is enhanced due to the existence of temperate ice and water at the base.

The combined freshwater production due to melting and calving vary in step with the climate forcing. There are peaks at 27 ka ago ($9200 \times 10^3\,\mathrm{km}^3\,\mathrm{year}^{-1}$), 22 ka ago ($6300 \times 10^3\,\mathrm{km}^3\,\mathrm{year}^{-1}$), lower but wider peaks at 19–18.5 ka ago ($3800 \times 10^3\,\mathrm{km}^3\,\mathrm{year}^{-1}$), 14 ka ago ($8300 \times 10^3\,\mathrm{km}^3\,\mathrm{year}^{-1}$) and finally a small peak at around 11–10 ka ago.

The areal extent of the ice sheet changes continually through the simulation. Maxima in the ice-covered area occur at 35 ka, 27–25 ka and 22–21 ka ago ($8.5 \times 10^6\,\mathrm{km}^2$). The

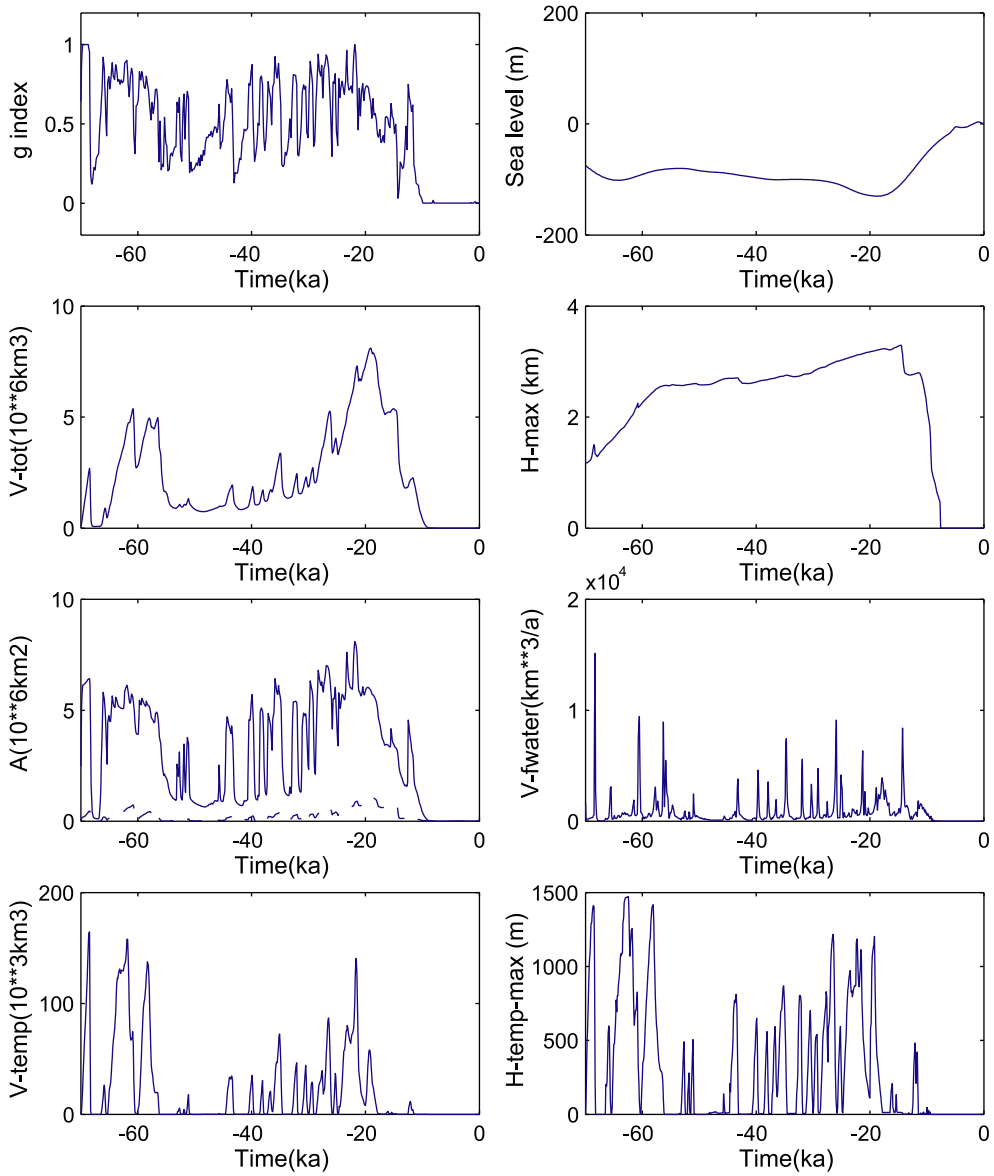

Figure 7: Forcings and results for simulation #1 (primary approach) as functions of time: glacial index, sea level, ice volume, maximum ice thickness, ice-covered area (solid line) and area covered by temperate ice (dotted line), freshwater production due to melting and calving, volume of temperate ice, maximum thickness of the temperate layer.

maximum volume at 19–18 ka ago is accompanied by a smaller areal extent ($6 \times 10^6\,\mathrm{km}^2$). Ice-cover maxima with thinner ice peaks at LGM, and the volume growth after that are presumably caused by increasing precipitation as the temperatures rise.

Not presented in the summarising figure, the maximum ice-sheet thickness of 3.3 km occurs at 17.3 ka ago, but values above 3.0 km are reached from 19.3 ka ago on. The ice sheet gradually declines, and the final disintegration starts after the Younger Dryas, near 10 ka ago.

4.2 Cold-ice mode (simulation #2)

The importance of including polythermal ice processes is tested by re-running the primary set-up with a cold-ice only model. In this case, the Stefan-type conditions at the transition surface between cold ice and temperate ice (which occurs typically in thin layers at the base) are ignored. Where heat balance would yield temperatures above the melting-point, the ice temperature is re-set to the pressure melting point.

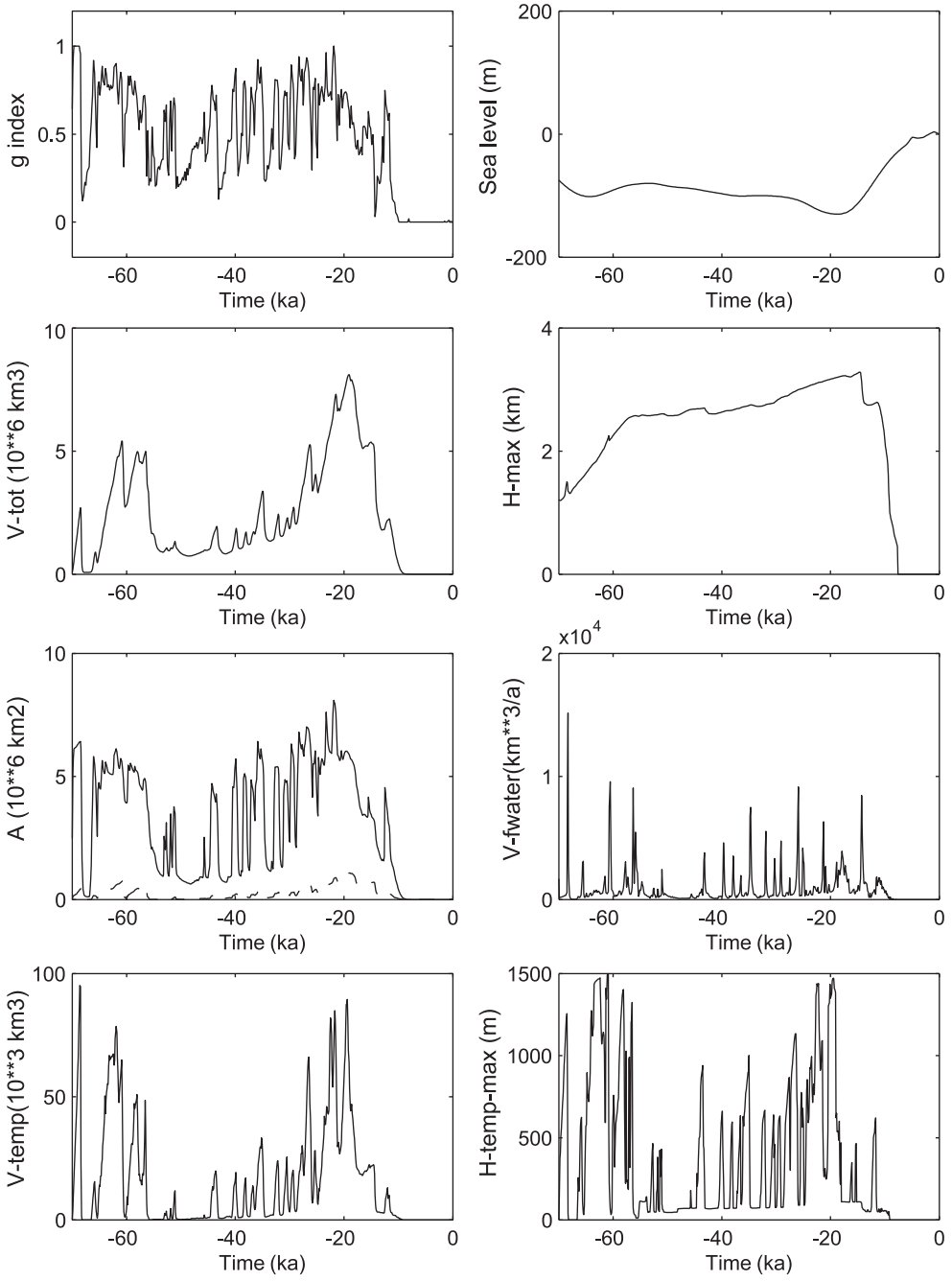

Figure 8: Like Fig. 7, but for simulation #2 (cold-ice mode).

The results for the cold-ice mode are summarized in Fig. 8. The main features of the polythermal and cold-ice models are very similar. The ice-sheet volume tends to be slightly larger in the cold-ice-mode until the deglaciation phase. The same pattern applies to areal extent. The implication is that the main restrictions to the ice-sheet growth are the topography and the climate forcing. The freshwater production peaks occur in the same time periods as in the primary approach, and with nearly identical values.

4.3 Different PDD factors (simulations #3 and #4)

We compare here model runs with the two extreme degree factors for ice, $\beta_{\text{ice}} = 5\,\text{mm w.e. day}^{-1}\,^{\circ}\text{C}^{-1}$ and $12\,\text{mm w.e. day}^{-1}\,^{\circ}\text{C}^{-1}$. The results are displayed in Fig. 9. The volumetric and areal features of the ice sheet are similar to the primary run, with similar timing of freshwater production due to melting and calving. The peak magnitudes are a little lower with the maximum ablation values. It seems that especially the SIS is very sensitive to the PDD factors during the deglaciation phase.

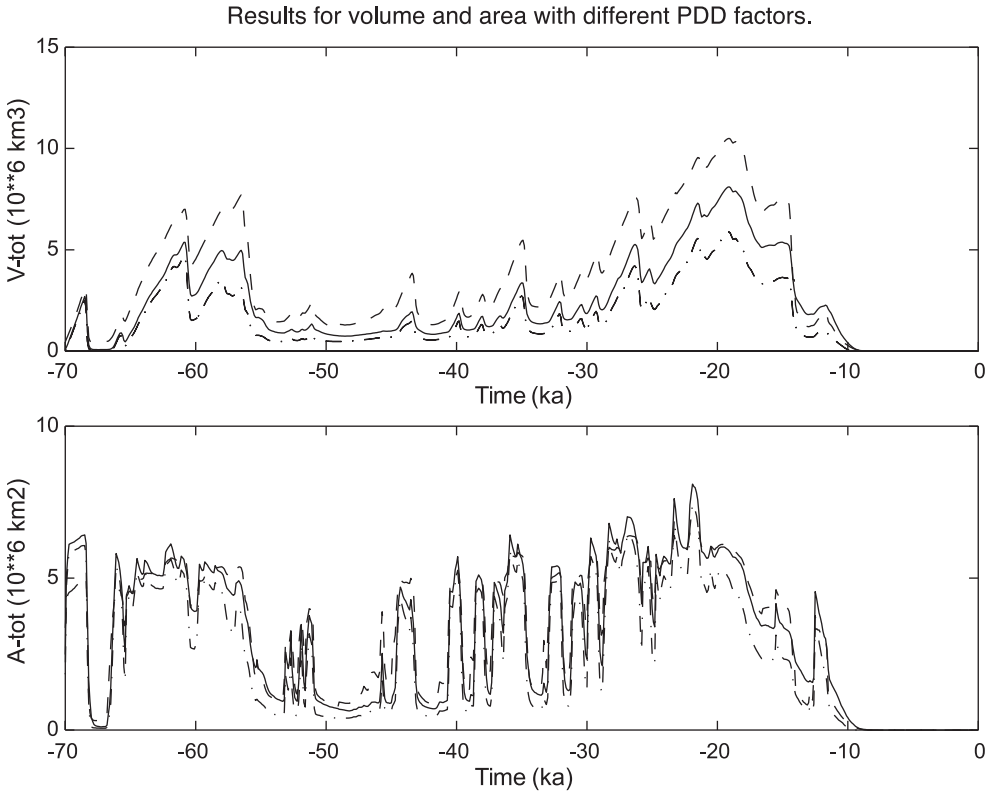

Figure 9: Ice volume and ice-covered area as functions of time for simulations #1 ($\beta_{\text{ice}} = 7\,\text{mm w.e. day}^{-1}\,^{\circ}\text{C}^{-1}$, solid), #3 ($\beta_{\text{ice}} = 5\,\text{mm w.e. day}^{-1}\,^{\circ}\text{C}^{-1}$, dashed) and #4 ($\beta_{\text{ice}} = 12\,\text{mm w.e. day}^{-1}\,^{\circ}\text{C}^{-1}$, dash-dotted).

The ice sheets resulting from our models are very sensitive to variations in ablation. Simulation #3 (low value of β_{ice}) strongly influences SIS and BIIS growth and decay, leading to a glaciation history that more resembles the QUEEN project outcome. The BIIS is still very modest, but persists for some thousands of years near the LGM. The BIS ice dome is slightly higher than for the primary model. Simulation #4 (high value of β_{ice}) causes a thinner BIS, which is in accordance to the QUEEN results. The SIS is overly small in extent and volume.

From Fig. 9 we conclude that a reduction of the degree-day factor has a stronger impact on ice sheet volume than an increase does. The implication is that in western areas, reducing ablation is the key to a more extensive glaciation.

4.4 Modified precipitation and temperature (simulations #5 and #6)

Both modified climatologies improve some aspect of the simulated ice sheet. Simulation #5 (reduced LGM precipitation) (Section 3.3) yields ice-sheet configuration in good general agreement with the QUEEN reconstruction. An exception is a somewhat too small SIS. The main ice domes form over the Barents Sea and Scandinavia. The volume of the ice sheet as well as the maximum ice-sheet thickness stay lower than estimated by several authors (Elverhoi et al., 1993; Lambeck, 1995; Peltier, 1994). The Barents sea remains partially open, and the BIS is limited to the east coast of Novaya Zemlya. Ice sheet extent at 22 ka ago is shown in Fig. 5, and the evolution of the glaciation from that time to 12 ka ago is depicted in Fig. 6, lower row. Other model parameters are summarized in Fig. 10. The pulses of freshwater have the same timing as in the primary approach. The flux is of course smaller as the area and volume are smaller.

Simulation #6 (Kageyama anomalies) produces an ice sheet geometry that agrees very well with the QUEEN data for the LGM. The areal extent is shown in Fig. 5. In this simulation, the extent and volume of both the SIS and the BIIS have a maximum around 22 ka ago. The elusive BIIS reaches significant size in this model run, originating from 26 ka ago, and having a maximum surface elevation of 2 km at 21.5 ka ago.

The LGM time period is also characterized by a high mass fluxes in western sites of paleo ice streams. A considerable mass flux prevails for the NCIS area, Norwegian coast, Storfjorden and Bear Island trough. At 17 ka ago, the mass flux peaks in the Storfjorden and Bear Island region. This is also the time when the British Isles ice sheet has disintegrated. The mass flux continues in the sites of paleo ice streams until 14 ka, when the SIS has completely disintegrated. Peaks in meltwater production correspond to both climate and ice-sheet discharge events. The freshwater flux is continuously high from

20 to 15 ka ago. The high peak between 15 and 14 ka ago is caused by the SIS melting. At 13 ka ago the SIS starts to grow again, as does the BIS. But the SIS retreats rapidly as the climate warms, and disappears at about 11 ka ago, which is not in accordance with observations. The BIS disintegrates at 8 ka ago.

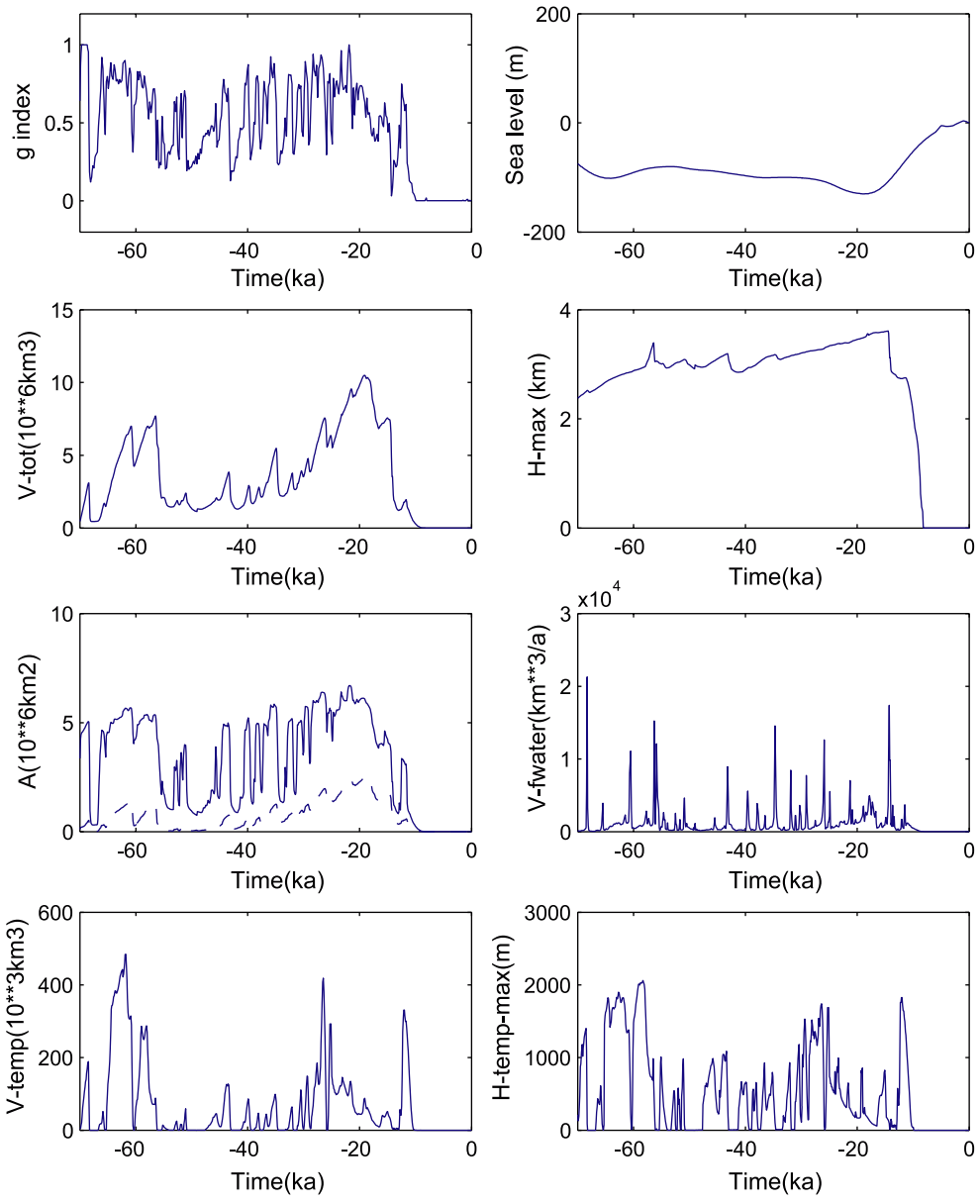

Figure 10: Like Fig. 7, but for simulation #6 (Kageyama anomalies).

5 Discussion

In our simulations, the main ice volume in Late Weichselian is concentrated in the Scandinavian and Barents area. The sea level minima coincides with ice sheet volume maxima. The maximum ice-sheet volume is reached at 19–18 ka ago, and there are small peaks at 35 and 27 ka ago. Nevertheless, the maximum volume does not coincide with the maximum extent. In all the model simulations, maximum extent has been reached near LGM and maximum volume about a thousand years after. After the LGM, the dome located in Fenno-Karelia starts to grow as the western section shrinks. The dome is largest around 19.5 ka ago. The center of the dome shifts slowly towards west, and at 18 ka ago it has a center over the Gulf of Bothnia. Comparing this to the different timings for LGM by QUEEN, our model simulations capture very well this feature with both the primary set-up (simulation #1) and the modified Kageyama climate (simulation #6). Especially, the latter simulations reproduce nicely the dynamics of different local LGMs, and show coherent, repetitive advances at a millennial time scale.

5.1 Deglaciation

Glacial-maximum ice-sheet volumes shrink shortly after 18 ka ago in all our model runs. Deglaciation proceeds in three stages, with stasis periods at 17–15 and 13–12 ka ago. After 10 ka ago, the ice sheets are gone.

The simulated deglaciation can be compared to simulation done by others (Charbit et al., 2002; Siegert et al., 1999). Our simulations underestimate ice volume, compared to Charbit et al. (2002), by ca. $2 \times 10^6\,\mathrm{km}^3$, but show similarities in deglaciation features with their GRIP-driven simulations. The stasis periods are more pronounced in our simulation results. This might be due to the late volume maximum in their results, at 15 ka ago. Their final disintegration takes place at 7 ka ago, and compared to our runs shows better agreement with observational data. This may be due to two reasons: the bigger ice volume and the inclusion of AGCM results in the forcing for 15, 9 and 6 ka ago, in contrary to the linear interpolation used in our runs.

5.2 Freshwater production

Freshwater is produced in our simulation runs by surface melting and calving. The melting is of course larger if the climate is warmer or the precipitation in warm areas is higher. Freshwater production varies significantly over the glacial cycle with pronounced discharge events. These peaks coincide with climate-warming events, but not all climate events produce proportionally equivalent fluxes. For example, in simulation #1 (primary approach),

the warming at 27 ka ago produces a water flux of 8000 $km^3\,year^{-1}$, while larger warming events at 35 and 15 ka ago contribute only 6000 $km^3\,year^{-1}$ of water.

The combined surface melting and calving effects dominate the total freshwater production. They contribute over 99% to the total water flux. These sources also tend to produce well-defined events, lasting about 500 years. Water produced by basal melt and drainage from temperate ice contribute about 0.2% and 0.1%, respectively, to the total flux. These two are clearly of minor importance to the total flux. These sources also vary over time, but produce relatively broad peaks, about 2000 years for basal melt and 1000 years for drainage from temperate ice. This is to be expected, as the basal ice must warm before it can flow fast and increase calving.

5.3 Fast flow and basal conditions

Fast, ice-stream-like flow takes place in regions with a temperate base and temperate ice above. Here, we are concerned with fast flowing outlets to the marine margins of ice sheets, which may play a role in Heinrich events.

In the simulation #1 (primary approach) and #5 and #6 (modified LGM climate anomalies), the western BIS has a temperate base with temperate ice above. Simulation #1 also produces temperate base areas with temperate ice above on the western Norwegian coastal areas, but only a small area with a temperate base in the NCIS. In simulation #6, the BIIS has a temperate base with temperate ice above for the largest part of its existence. Basal conditions for simulation #6 at 26.7, 22.0 and 20.4 ka ago are presented in Fig. 11. In the southwest sector of the SIS, there is a large temperate base and temperate ice area, and also on the Norwegian coast. As a fast flow in the NCIS area sets on, e.g., at 22 ka ago, first the temperate base area expands to the Kattegat area on the Swedish coast, around 23 ka ago. In a later phase, temperate basal conditions can be seen in the Baltic area, but as these are not connected to marine fast flow areas, they are not discussed here. The relatively rapid draw-down allows the ice sheet to quickly recover from the volume loss of fast flow event in the NCIS.

5.4 Comparison with IRD events

In all our model results, there are freshwater pulses from melting and calving at 27, 22, 19–18.5, 14 and 11–10 ka ago. These correspond with HEs except for the peak at 19–18.5 ka ago. However, this agreement must be taken with some care because (1) only large calving events as a consequence of fast flow contribute to debris discharge into the ocean (whereas pure melting events do not), and (2) debris discharge rates need not be proportional to

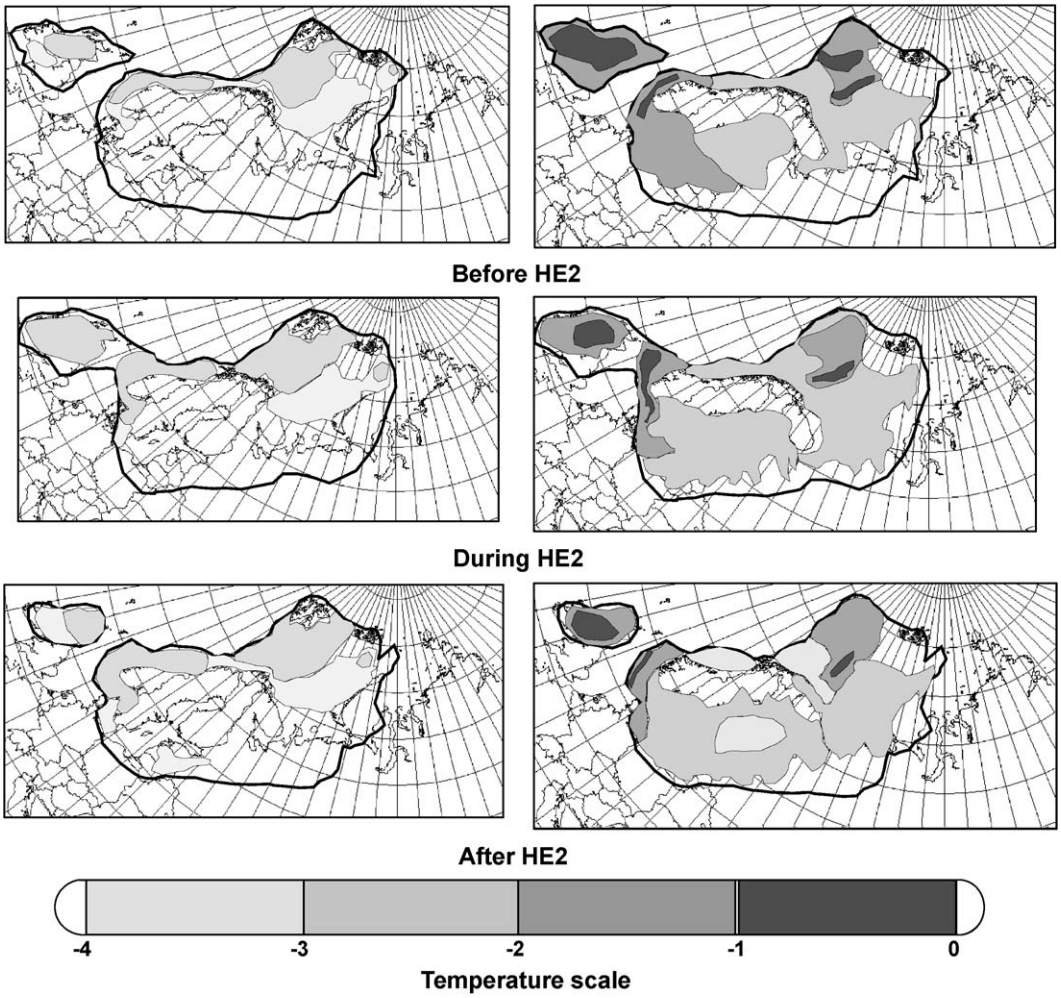

Figure 11: Basal conditions before, during and after HE2 for simulation #6 (Kageyama anomalies). The left panels depict the temperate base with temperate ice above (darker shading) and the temperate base with cold ice above (lighter shading). The right panels show the basal temperate, with the darkest values just below zero. The exact dates for these pictures are 26.7, 22.0 and 20.4 ka ago.

iceberg discharge rates for all times (see for instance the discussion by Alley and MacAyeal (1994)). Therefore, we will now discuss the simulated freshwater pulses in more detail.

First, it is evident that for all simulations the temporal evolution of the ice-covered area is more spiky than that of the ice volume in the vicinity of the modelled freshwater pulses (Figs. 7-10). This is so because a large area of ice-free land can turn into an area covered by a thin ice layer (and vice-versa) within a very short time when climate conditions change accordingly. By contrast, considerable volume changes, either rapidly decrease due to a melting/calving event or rapidly increase afterwards due to ice accumulation (snowfall) and glacial flow, require naturally more time.

We now focus on three of the model runs. Simulations #1 (primary approach) and #3 (reduced β_{ice}) yield similar scenarios. The flux peak at 27 ka results from the ice sheet reaching its maximum extent on the continental slope. The NCIS and Storfjorde are active, but large volume fluxes can be seen in Franz Victoria Trough area. At 22 ka, the reason for the freshwater flux is the maximum extent on the continental slope, with high ice volume fluxes at the NCIS, Voring Plateau and Franz Victoria Trough. At 14 ka the SIS melts away, resulting in a large meltwater flux through Bear Island Trough. 11 ka marks the final disintegration of the BIS, and results in large volume fluxes in the Franz Victoria Trough.

For simulation #6 (Kageyama anomalies), the discharge history is distinctly different. The flux peak at 27 ka has the same cause as in the other two runs, and the NCIS is very active. At the LGM, the ice sheet extends to the continental margin as deep as we allow it to glaciate. The NCIS flows fast, but ice-stream activity is moderate elsewhere. As the NCIS transports ice fast to the coastal calving area, the western section of the ice sheet thins. This simulation thus differs from those mentioned above over the time period from 18 to 14 ka, which is marked with several active fast flow areas. Volume fluxes trough the Bear Island Trough remain large through this period. In the central Norwegian Voring Plateau, there is a peak in volume flux at 18–16.5 ka ago. At 14 ka the SIS melts away, with increased fluxes at Central Norway, Storfjorden and Bear Island Trough. 11 ka marks the final disintegration of BIS. Our results indicate an active NCIS at HE3 and HE2, and the activity then shifting to northern fast flow areas. The different temporal and spatial distributions of fast flow regions from the LGM to the Holocene are summarized in Table 6 for the simulations #1 and #6.

Simulation	NCIS	Central Norway	Bear Island and Storfjorden	Franz Victoria Trough
#1	$\sim$27	$\sim$27, $\sim$22	$\sim$17–14	$\sim$27
	$\sim$22	$\sim$19–18		$\sim$22–9
#6	$\sim$27–26	$\sim$18–16.5	$\sim$18–14	$\sim$22–9
	$\sim$22–20			

Table 6: Main fast flow areas and their timing (age in ka), for simulations #1 (primary approach) and #6 (Kageyama anomalies).

Elliot et al. (2001) conclude that the IRD contents in sediment cores indicate that Northern Hemisphere ice sheets send forth iceberg armadas at the same time during HEs. These records also reveal that inter-HEs operate mainly on the nordic regions, and in the Norwegian Sea well-defined layers of high IRD-content are present close to glacier outlet areas at cold stadials. It seems thus that the Fennoscandian Ice Sheet may have been very

sensitive to climate forcing, and could have responded quickly to changes in climate, like the modes of the North Atlantic Oscillation (NAO).

Dreger (1999) studied several sediment cores in the North sea area. The cores MD95-2011 (near Voring plateau) and MD95-2012 (near Bear Island Trough) reveal high sedimentation and bulk accumulation rates in deglaciation. Around 16.7–16.6 ka there are high values in the MD95-2011, and there is a lower peak at 18.7–18.9 ka. For the MD95-2012, there are high values from 15.9 to 15.7 ka and lower peak value from 17.9 to 17.3 ka ago.

Our simulation results are in agreement with these findings, in particular simulation #6. The Kageyama temperature anomalies applied for this simulation are more pronounced in the Scandinavian area than the UKMO21 anomalies used for the other simulations, so that the temperature effect on coastal Norwegian Sea areas is enhanced. There are repetitive advances of the ice sheets, characterized by high ice volume fluxes. Fast-flow areas on the western margin transport ice to the coast but recover fast from ice volume pulses. The simulation results display freshwater fluxes from melting and calving in phase with Heinrich events H3 at 27, H2 at 22, and H1 at 14 ka ago. These peaks correspond to fast flow areas, with main activity at 27 and 22 ka ago in the Nordic Channel area and later in the Bear Island and Storfjorden region. The activity of these areas seems to be shifting from south to north from the LGM to the Holocene. The freshwater pulse at 19–18.5 ka could correspond to a Dansgaard-Oeschger oscillation, as well as the ice volume flux peaks around 18–17 ka ago on the western margin of the ice sheet. In a more detailed analysis of our results of Norwegian coastal areas, we have similar peaks and one extra than in the study of Dreger (1999) in our ice volume flux history. For the Voring Plateau, these simulated peaks occur at 18.0–17.7, 17.5–17.0 and 16.8–16.6 ka ago. In the Bear Island regions, our simulations indicate high volume fluxes from 17.8, 17.5 and from 17.2 to 14.2 ka ago.

6 Conclusion

The areal extent and ice-stream locations of the Eurasian glaciation are simulated rather well with our primary set-up simulation. However, the volume of the ice sheet remains too low. This in consequence leads to a too fast deglaciation. By applying modified LGM temperature and precipitation anomalies, the results become consistent with the QUEEN reconstruction for the Eurasian ice sheet extent. In order to improve the simulation of the deglaciation chronology, GCM temperature and precipitation anomalies for 15, 9 and 6 ka ago should be utilized as additional time-slices for pinning the climate interpolation.

The results suggest areal and temporal variations in fast-flow areas which were already discussed by Forsström et al. (2003). The forming ice sheets are very sensitive and respond

fast to changes in temperature and precipitation. The peaks in freshwater discharge are coinciding in all the runs, and the volume of the ice sheet and the climatic conditions determine the freshwater flux. Most freshwater peaks can be correlated to the observed occurrence of Heinrich Events (HE), and one to Dansgaard-Oeschger (D-O) oscillations. Other connections to D-O oscillations can be drawn from the ice volume flux peaks around 18–17 ka ago. The areal occurrence of ice streams seems to be shifting from south to north with ongoing time.

Acknowledgements

The authors express their gratitude to M. Saarnisto (Geological Survey of Finland) for valuable suggestions. O. Sallasmaa is thanked for preliminary manipulation of climate data. We appreciate and gratefully recognize the helpful suggestions and comments of referees T. Hughes and C. Hulbe. The resources of the Center for Scientific Computing in Finland made this study possible.

References

Alley, R.B., Clark, P.U., 1999. The deglaciation of the northern hemisphere: a global perspective. Annu. Rev. Earth Planet. Sci. 27, 149–182.

Alley, R.B., MacAyeal, D.R., 1994. Ice-rafted debris associated with binge/purge oscillations of the Laurentide ice sheet. Paleoceanography 9 (4), 503–511.

Blankenship, D.D., et al., 1993. Active volcanism beneath the West Antarctic Ice Sheet and implications for ice-sheet stability. Nature 361, 526–529.

Bond, G.C., Lotti, R., 1995. Iceberg discharges into the North Atlantic on millennial time scales during the last glaciation. Science 267, 1005–1010.

Bond, G., Heinrich, H., Broecker, W., Labeyrie, L., McManus, J., Andrews, J., Huon, S., Jantschik, R., Clasen, S., Simet, C., Tedesco, K., Klas, M., Bonani, G., Ivy, S., 1992. Evidence for massive discharges of icebergs into the North Atlantic ocean during the last glacial. Nature 360, 245–249.

Bond, G., Broecker, W., Johnsen, S., McManus, J., Labeyrie, L., Jouzel, J., Bonani, G., 1993. Correlations between climate records from North Atlantic sediments and Greenland ice. Nature 365, 143–147.

Boulton, G.S., Dongelmans, P., Punkari, M., Broadgate, M., 2001. Palaeoglaciology of an ice sheet through a glacial cycle: the European ice sheet through the Weichselian. Quat. Sci. Rev. 20, 591–625.

Braithwaite, R.J., 1995. Positive degree-day factors for ablation on the Greenland ice sheet studied by energy-balance modelling. J. Glaciol. 41 (137), 441–444.

Calov, R., Ganopolski, A., Petoukhov, V., Claussen, M., Greve, R., 2002. Large-scale instabilities of the Laurentide ice sheet simulated in a fully coupled climate-system model. Geophys. Res. Lett. 29 (24), 2216 (doi:10.1029/2002GL016078).

Charbit, S., Ritz, C., Ramstein, G., 2002. Simulations of Northern Hemisphere ice-sheet retreat: sensitivity of physical mechanisms involved during the Last Deglaciation. Quat. Sci. Rev. 21, 243–265.

Clark, P.U., Alley, R.B., Pollard, D., 1999. Northern hemisphere ice-sheet influences on global climate change. Science 286, 1103–1111.

Clark, P.U., Pisias, N.G., Stocker, T.F., Weaver, A.J., 2002. The role of the thermohaline circulation in abrupt climate change. Nature 415, 863–869.

Dansgaard, W., Clausen, H.B., Gundestrup, N., Hammer, C.U., Johnsen, S.F., Kristinsdottir, P.M., Reeh, N., 1982. A new Greenland deep ice core. Science 218, 1273–1277.

Dansgaard, W., Johnsen, S.J., Clausen, H.B., Dahl-Jensen, D., Gundestrup, N.S., Hammer, C.U., Hvidberg, C.S., Steffensen, J.P., Sveinbjörnsdottir, A.E., Jouzel, J., Bond, G., 1993. Evidence for general instability of past climate from a 250-kyr ice-core record. Nature 364, 218–220.

Dreger, D., 1999. Decadal-to-Centennial-Scale Sediment Records of Ice Advance on the Barents Shels and Meltwater Discharge Into the Northeastern Norwegian Sea Over the Last 40 kyr. Dissertation to Christian-Albrechts-Universität, Kiel.

Elliot, M., Labeyrie, L., Bond, G., Cortijo, E., Turon, J.L., Tisnerat, N., Duplessy, J.C., 1998. Millennial-scale iceberg discharges in the Irminger Basin during the last glacial period: relationship with the Heinrich events and environmental settings. Paleoceanography 13, 433–446.

Elliot, M., Labeyrie, L., Dokken, T., Manthè, S., 2001. Coherent pattern of ice-rafted debris deposits in the Nordic regions during the last glacial (10–60 ka). Earth Planet. Sci. 194, 151–163.

Elverhoi, A., Fjedskaar, W., Solheim, A., Nylandberg, M., Rasswurm, L., 1993. The Barents Sea Ice Sheet – a model of its growth and decay during the last ice maximum. Quat. Sci. Rev. 12, 863–873.

Engelhardt, H., Kamb, B., 1997. Basal hydraulic system of a West Antarctic ice stream: constraints from borehole observations. J. Glaciol. 43, 207–244.

Fairbanks, R.G., 1989. A 17000-year glacio-eustatic sea level record; influence of glacial melting rates on the Younger Dryas event and deep-ocean circulation. Nature 342, 637–642.

Fastook, J., Holmlund, P., 1994. A glaciological model of the Younger Dryas event in Scandinavia. J. Glaciol. 40 (134), 125–132.

Forsström, P.-L., Sallasmaa, O., Greve, R., Zwinger, T., 2003. Simulation of fast-flow features of the Fennoscandian ice sheet during the Last Glacial Maximum. Ann. Glaciol. 37, 383–389.

Fowler, A.C., Johnson, C., 1995. Hydraulic runaway: a mechanism for thermally regulated surges of ice sheets. J. Glaciol. 41, 554–561.

Ganopolski, A., Rahmstorf, S., 2001. Rapid changes of glacial climate simulated in a coupled climate model. Nature 409, 153–158.

Giorgi, F., Marrinucci, M.R., Bates, G.T., 1993a. Development of a second generation regional climate model (RegCM2): Part I. Boundary-layer and radiative transfer processes. Mon. Weather Rev. 121, 2794–2813.

Giorgi, F., Marrinucci, M.R., Bates, G.T., 1993b. Development of a second generation regional climate model (RegCM2): Part II. Convective processes and assimilation of lateral boundary conditions. Mon. Weather Rev. 121, 2814–2832.

Greve, R., 1997a. A continuum-mechanical formulation for shallow polythermal ice sheets. Philos. Trans. R. Soc. Lond., A 355, 921–974.

Greve, R., 1997b. Application of a polythermal three-dimensional ice sheet model to the Greenland ice sheet: response to steady-state and transient climate scenarios. J. Climate 10 (5), 901–918.

Greve, R., 2001. Glacial isostasy: models for the response of the Earth to varying ice loads. In: Straughan, B., Greve, R., Ehrentraut, H., Wang, Y. (Eds.), Continuum Mechanics and Applications in Geophysics and the Environment. Springer, Berlin, pp. 307–325.

Greve, R., Weis, M., Hutter, K., 1998. Palaeoclimatic evolution and present conditions of the Greenland Ice Sheet in the vicinity of Summit: an approach by large-scale modelling. Paleoclimates 2 (2–3), 133–161.

Hagen, J.O., Melvold, K., Eiken, T., Isaksson, E., Lefauconnier, B., 1999. Mass balance methods on Kongsvegen, Svalbard. Geogr. Ann., Ser. A 81A (4), 593–601.

Heinrich, H., 1988. Origin and consequences of cyclic ice rafting in the northeast Atlantic Ocean during the past 130,000 years. Quat. Res. 29, 142–152.

Hewitt, C.D., Mitchell, J.F.B., 1997. Radiative forcing and response of a GCM to ice age boundary conditions: cloud feedback, and climate sensitivity. Clim. Dyn. 13 (11), 821–834.

Hulbe, C.L., MacAyeal, D.R., 1999. A new thermodynamical numerical model of coupled ice sheet, ice stream, and ice shelf flow. Journal of Geophysical Research, 104 (B11), 25, 349–366.

Hutter, K., 1993. Thermo-mechanically coupled ice-sheet response – cold, polythermal, temperate. J. Glaciol. 39 (131), 65–86.

Huybrechts, Ph., de Wolde, J., 1999. The dynamic response of the Greenland and Antarctic ice sheets to multiple-century climatic warming. J. Climate 12 (8), 2169–2188.

Huybrechts, Ph., T'siobbel, S., 1995. Thermomechanical modelling of northern hemisphere ice sheets with a two-level mass-balance parameterisation. Ann. Glaciol. 21, 111–116.

Imbrie, J., Hays, J.D., Martinson, D.G., McIntyre, A., Mix, A.C., J.J., J.J., Morley, J.J., Pisias, N.G., Prell, W.L., Shackleton, N.J., 1984. The orbital theory of Pleistocene climate: support from a revised chronology of the marine delta18O record. In: Berger, A., et al., (Ed.), Milankovitch and Climate, Part I. NATO ASI Series. Series C: Mathematical and Physical Sciences, vol. 126. D. Reidel Publishing, Dordrecht, Holland, pp. 269–305.

Johnson, J., Fastook, J.L., 2002. Northern Hemisphere glaciation and its sensitivity to basal melt water. Quat. Int. 95-96, 65–74.

Kageyama, M., Peyron, O., Pinot, S., Tarasov, P., Guiot, J., Joussame, S., Ramstein, G., 2001. The Last Glacial Maximum climate over Europe and western Siberia: a PMIP comparison between models and data. Clim. Dyn. 17, 23–43.

Kjaer, K.H., Demidov, I., Houmark-Nielsen, M., Laersen, E., 2001. Distinguishing between tills from Valdaian ice sheets in the Arkhangelsk region. Global and Planetary Change 1–4 (31), 201–214.

Kleman, J., Hättestrand, C., Borgström, I., Stroeven, A., 1997. Fennoscandian palaeoglaciology reconstructed using a glacial geological inversion model. J. Glaciol. 43 (144), 283–299.

Knies, J., Kleiber, H.-P., Matthiessen, J., Miller, C., Nowaczyk, N., 2001. Marine ice-rafted debris records constrain maximum extent of Saalian and Weichselian ice-sheets along the northern Eurasian margin. Glob. Planet. Change 31 (1–4), 45–64.

Koç, N., Jansen, E., 1992. A high resolution diatom record of the last deglaciation from the SE Norwegian Sea: documentation of rapid climatic changes. Paleoceanography 7, 499–520.

Lambeck, K., 1995. Constraints of the Late Weichselian Ice Sheet over the Barents Sea from Observations of raised shorelines. Quat. Sci. Rev. 14, 1–16.

Larsen, E., Lysså, A., Demidov, I., Funder, S., Houmark-Nielsen, M., Kjaer, K.H., Murray, A.S., 1999. Age and extent of the Scandinavian ice sheet in northwest Russia. Boreas 28, 115–132.

Legates, D.R., Wilmott, C.J., 1990. Mean seasonal and spatial variability in global surface air temperature. Theor. Appl. Climatol. 41, 11–21.

LeMeur, E., Huybrechts, P., 1996. A comparison of different ways of dealing with isostasy: examples from modelling the Antarctic ice sheet during the last glacial cycle. Ann. Glaciol. 23, 309–317.

Lunkka, J.P., Saarnisto, M., Gey, V., Demidov, I., Kiselova, V., 2001. Extent and age of the Last Glacial Maximum in the south-eastern sector of the Scandinavian Ice Sheet. Glob. Planet. Change 31 (1–4), 407–425.

Mangerud, J., Astakov, V., Svendsen, J.-I., 2002. The extent of the Barents-Kara ice sheet during the Last Glacial Maximum. Quat. Sci. Rev. 21 (1–3), 111–119.

Marshall, S.J., Clarke, G.K.C., 1999. Ice sheet inception: subgrid hypsometric parameterization of mass balance in an ice sheet model. Clim. Dyn. 15 (7), 533–550.

Marshall, S.J., Tarasov, L., Clarke, G.K.C., Peltier, W.R., 2000. Glaciological reconstruction of the Laurentide Ice Sheet: physical processes and modelling challenges. Can. J. Earth Sci. 37 (5), 769–793.

Marsiat, I., 1994. Simulation of the northern hemisphere continental ice sheets over the last glacial-interglacial cycle: experiments with a latitude-longitude vertically integrated ice sheet model coupled to zonally averaged climate model. Palaeoclimates 1, 59–98.

Payne, A.J., Baldwin, D.T., 1999. Thermomechanical modelling of the Scandinavian Ice Sheet: implications for ice stream formation. Ann. Glaciol. 28, 83–89.

Peltier, W.R., 1994. Ice age palaeotopography. Science 256, 195–201.

Peyron, O., Guiot, J., Cheddadi, R., Tarasov, P., Reille, M., Beauheid, J.K., de Bottema, S., Andrieu, V., 1998. Climatic reconstruction in Europe for 18,000 yr B.P. from pollen data. Quat. Res. 49, 183–196.

Pollard, D., Barron, E.J., 2003. Causes of model-data discrepancies in European climate during oxygen isotope stage 3 with insights from the last glacial maximum. Quat. Res. 59, 108–113.

Pollard, D., PMIP Participating Groups, 2000. Comparisons of ice-sheet surface mass budgets from Paleoclimate Modeling Intercomparison Project (PMIP) simulations. Glob. Planet. Change 24 (3–4), 79–106.

Polyak, L., Levitan, M., Gataullin, V., Khusid, T., Mikhailov, V., Mukhina, V., 2000. The impact of glaciation, river discharge and sea-level change on Late Quaternary environments in the southwestern Kara Sea. Int. J. Earth Sci. 89 (3), 550–562.

Raymond, C.F., 2000. Energy balance of ice streams. J. Glaciol. 46 (155), 665–674.

Reeh, N., 1991. Parameterization of melt rate and surface temperature on the Greenland Ice Sheet. Polarforschung 59 (3), 113–128.

Saarnisto, M., Lunkka, J.P., 2002. Climate variability during the last interglacial-glacial cycle in NW Eurasia. In: Battarbee, R., Gasse, F., Stickley, C. (Eds.), Past Climate Variability through Europe and Africa. Kluwer Academic Publisher, Dordrecht. In press.

Sejrup, H.P., Landvik, J.Y., Larsen, E., Janocks, J., Eiriksson, J., King, E., 1998. The Jaeren area, a border zone of the Norwegian Channel Ice Stream. Quat. Sci. Rev. 17 (9–10), 801–812.

Sejrup, H.P., Larsen, E., Landvik, J.Y., King, E.L., Haflidason, H., Nesje, A., 2000. Quaternary glaciations in southern Fennoscandia: evidence from southwestern Norway and the northern North Sea region. Quat. Sci. Rev. 19 (7), 667–685.

Siegert, M.J., Dowdeswell, J.A., Melles, J.A., 1999. Late Weichselian glaciation of the Eurasian Hight Arctic. Quat. Res. 53, 273–285.

Stocker, T.F., 2000. Past and future reorganisations in the climate system. Quat. Sci. Rev. 19, 301–319.

Stokes, C.R., Clark, C.D., 2001. Palaeo-ice streams. Quat. Sci. Rev. 20, 1437–1457.

Svendsen, J.I., Astakhov, V.I., Bolshiyanov, D.Y., Demidov, I., Dowdeswell, J.A., Gataullin, V., Hjort, C., Hubberten, H.W., Larsen, E., Mangerud, J., Melles, M., Möller, P., Saarnisto, M., Siegert, M.J., 1999. Maximum extent of the Eurasian ice sheets in the Barents and Kara Sea region during the Weichselian. Boreas 28, 234–242.

Tarasov, P.E., Peyron, O., Guiot, J., Brewer, S., Volkova, V.S., Bezusko, L.G., Dorofeyk, N.I., Kvavadze, E.V., Osipova, I.M., Panova, N.K., 1999. Last Glacial Maximum climate of the former Soviet Union and Mongolia reconstructed from pollen and plant microfossil data. Clim. Dyn. 15 (3), 227–240.

Thiede, J., Bauch, H.A., Hjort, C., Mangerud, J., 2001. The Late Quaternary Stratigraphy and Environments of Northern Eurasia and the Adjacent Arctic Seas – New Contributions from QUEEN. Glob. Planet. Change 31 (1–4) (complete volume), 479 pp.

Thompson, S.L., Pollard, D., 1997. Greenland and Antarctic mass balances for present and doubled atmospheric CO2 from the GENESIS version 2 global climate model. J. Climate 10, 871–900.

Tulaczyk, S., Kamb, B., Engelhardt, H., 2000a. Basal mechanics of Ice Stream B: I. Till mechanics. J. Geophys. Res. 105, 463–481.

Tulaczyk, S., Kamb, B., Engelhardt, H., 2000b. Basal mechanics of Ice Stream B: II. Plastic-undrained-bed model. J. Geophys. Res. 105, 483–494.

Van der Veen, C.J., 1999. Fundamentals of Glacier Dynamics, 1st edition. A.A. Balkema, Rotterdam.

Vose, R.S., Schmoyer, R.L., Steurer, P.M., Peterson, T.C., Heim, R., Karl, T.R., Eischeid, J.K., 1992. The global historical climatology network: long-term monthly temperature, precipitation, sea level pressure, and station pressure data. NDP-041 Carbon Dioxide Information Analysis Center. Oak Ridge National Laboratory, Oak Ridge, TN.